Nuclear morphogenesis: forming a heterogeneous nucleus during embryogenesis

Albert Tsai[1, †] & Justin Crocker[1,†].
1 European Molecular Biology Laboratory, Heidelberg, Germany
† Co-corresponding authors: A.T. albert.tsai@embl.de J.C. justin.crocker@embl.de

Summary statement

We observed spatial rearrangements in the nucleus during embryo development, progressively forming a heterogeneous nuclear environment, paralleling the increasing complexity of the embryo body as morphogenesis progresses.

Abstract

An embryo experiences progressively complex spatial and temporal patterns of gene expression that guide the morphogenesis of its body plan as it matures. Using super-resolution fluorescence microscopy in *Drosophila melanogaster* embryos, we observed a similar increase in complexity in the nucleus: the spatial distributions of transcription factors became increasingly heterogeneous as the embryo matured. We also observed a similar trend in chromatin conformation with the establishment of specific histone modification patterns. However, transcription sites of specific genes had distinct local preferences for histone marks separate from the average nuclear trend, depending on the time and location of their expression. These results suggest that reconfiguring the nuclear environment is an integral part of embryogenesis and that the physical organization of the nucleus is a key element in developmental gene regulation.

Introduction

During embryogenesis, transcriptional regulation controls the expression of genes that ultimately leads to the patterning of the animal (Long et al., 2016; Mallo and Alonso, 2013; Reiter et al., 2017; Spitz and Furlong, 2012). This regulatory process involves interactions between transcription factors, chromatin regulators, and

genome topology. Large-scale genome-wide assays have revealed a diversity of functional regulatory elements and the factors that bind them (Consortium, 2012; Johnson et al., 2007; Kundaje et al., 2015; Stunnenberg et al., 2016; Thurman et al., 2012). Notably, these assays have detected wide-ranging reorginizaitons within the nucleus during cellular differentiation, where longer range interactions may bring together chromatin regions and genes into Topologically Associated Domains (TADs). These observations suggest that cellular differentiation involves transforming a nucleus from a uniform compartment into a heterogeneous and partitioned space. However, these aggregate maps represent signals averaged over populations of cells and therefore mask cellular and regulatory heterogeneity. There is now recognition that cell-to-cell variation of transcription factors, chromatin modifications, and interactions between regulatory elements are critical for animal development (Furlong and Levine, 2018; Shema et al., 2019; Tanay and Regev, 2017). However, a significant challenge in the field has been to pair single-cell and gene techniques with complex tissues and devolpmental systems.

Improvements in imaging technology—including dyes, probes, resolution, and throughput—are advancing capabilities for measuring regulatory interactions in developmental systems at the single cell and locus level (Chen et al., 2018; Garcia et al., 2013; Lim et al., 2018; Mir et al., 2017, 2018; Tsai et al., 2017). These techniques can spatially resolve genome regulation at high resolution (Bintu et al., 2018; Mateo et al., 2019; Shema et al., 2019), opening the door to direct observations of the local transcriptional environments around individual gene loci in specific cells. We have previously found that the distributions of transcription factors are heterogeneous in nuclei of *Drosophila* embryos in a late stage of development and that genes such as *shavenbaby* (*svb*) reside in regions enriched for transcription factors when they are transcriptionally active (Tsai et al., 2017).

However, the origins and functional properties of these transcriptional microenvironments during development remain unclear. When do transcriptional microenvironment form in the nucleus? How are these microenvironments affecting transcriptional regulation? In this survey, we imaged the distributions of transcription factors and histone modifications in *Drosophila melanogaster* embryos at different stages of development. Additionally, we imaged histone modifications at *hunchback* and *rhoNEE* enhancer-driven transcription sites to follow how the regulatory preferences of a gene changes when it is expressed at different stages of embryo development and in different locations on the embryo. In sum, we found that specific nuclear environments are

51 associated with active transcription and that the nuclear space becomes progressively more heterogeneous as
52 development proceeds, paralleling macroscopic morphogenesis of the whole embryo. This change in nuclear
53 organization could alter the regulatory properties at different locations in the nucleus and times during
54 embryogenesis, facilitating increasingly complicated regulatory patterns in later stages of embryogenesis.

55 Results and Discussions

56 Transcription factor distributions become more heterogeneous as development
57 progresses

58 Hunchback (Hb) is a transcription factor that is active through multiple developmental stages. It is a
59 gap gene in the early embryo, establishing the classical pattern (Figure 1A) immediately following
60 cellularization (stage 5). Hb expression moved into neuroblasts (Figure 1B, stage 8) and eventually into the
61 ventral nerve cord (Figure 1C, stage 14) as the embryo matured. The overall pattern localized from a broad
62 pattern n the early embryo into individual nuclei of a specific cellular lineage. To investigate if the sub-nuclear
63 distribution of Hb also changes during development, we imaged Hb distributions in fields of nuclei across three
64 different developmental stages using high-resolution confocal microscopy with AiryScan and super-resolution
65 STED microscopy. At stage 5 (Figure 1D), Hb was uniformly distributed across the entire nucleus. At stage 8
66 (Figure 1E), Hb began to show distinct nuclear regions of higher and lower concentrations. At stage 14 (Figure
67 1F), this heterogeneity has progressed further, with regions of very high Hb concentration (similar to that of
68 stage 5) juxtaposed next to regions with almost no Hb.

69 To quantify the spatial distributions of Hb, we computed the autocorrelation of Hb intensity (Figure
70 1G). The levels of correlation at a given length indicates spatial structures/features at that length scale. There
71 was a monotonous increase in the level of correlation as the embryo ages, suggesting that localized Hb
72 concentrations spanning several hundred nanometers became more prevalent as development proceeded. We
73 also imaged Krüppel (Kr) distributions across similar developmental stages and computed their autocorrelation

74 functions (Figure S1A). There was also a general upward trend, suggesting the formation of local transcription
75 factor environments.

76 Other transcription factors active within a limited time frame during development, such as
77 Ultrabithorax (Ubx, Figure S1B) and Engrailed (En, Figure S1C) showed high autocorrelation between when
78 they are first expressed and when they reach maximum expression in the nuclei of cells in the ectoderm (stage
79 10 until stage 14, using STED imaging). Their autocorrelation functions decreased at stage 16, when the cells
80 no longer expressed them and their distributions became very sparse. In sum, the nuclear distributions of Hb
81 and Kr, which are active from early to late developmental stages, went from uniform to heterogeneous,
82 whereas distributions of transcription factors (Ubx and En) that are only active later during development only
83 showed the latter pattern.

84 Localized histone modifications become established during development

85 Because transcription factors interact with the chromatin, we suspected that the state of the
86 chromatin would influence where these factors localize. Several works have associated active regions of the
87 chromatin with more open conformations, whereas repressed chromatin tend to be condensed (Boettiger et
88 al., 2016; Szabo et al., 2018)(Figure S1D). We therefore imaged the distributions of several histone
89 modifications associated using high-resolution confocal microscopy to track how their spatial distributions
90 change as embryos age. We imaged in regions showing transcription sites from a reporter construct driven by
91 the *hunchback* (*hb*) *cis*-regulatory region (*hbBAC*, see "Fly lines" in Materials and methods). We imaged
92 embryos at stages 5 and 10, where nuclei transcribing from the *hbBAC* construct are within 20 µm of the
93 surface of the embryo to preserve optimal optical resolution. We stained for H3K4me1 (Figure 2A, enhancers),
94 H3K4me3 (Figure 2B, promoters), H3K27ac (Figure 2C, active promoters and enhancers), H3K36me3 (Figure
95 2D, active gene bodies) and H3K27me3 (Figure 2E, transcriptionally repressed regions).

96 In general, the trend was an increasing amount of histone modifications as the embryo aged from
97 stage 5 to 10 (Figure 2A-E). The most drastic increase was with H3K27me3, which went from barely detectible
98 to condensed regions of very high intensities. The autocorrelation functions of the histone modifications in
99 Figure 2F-J showed that histone marks also became more spatially expansive, with all marks showing increased

100 correlation across all length scales. H3K27me3 (Figure 2J) showed the largest amount of change followed by
101 H3K4me3 (Figure 2G). Overall, histone modifications became established and more heterogeneous in older
102 embryos, but repressive modifications showed the most striking increase.

103 Temporally dependent changes in the levels of histone modifications around *hunchback* 104 transcription sites

105 The changing histone modification patterns during embryogenesis could alter the chromatin
106 environments around genes active across multiple developmental stages, such as *hunchback* (*hb*). We
107 therefore imaged how the levels of different histone modifications around *hb* transcription sites change in
108 embryos of two different ages. To obtain strong fluorescence signals for histone modifications using
109 immunofluorescence (IF) staining, we employed a method that does not require the denaturing step in RNA
110 fluorescence *in situ* hybridization (RNA FISH) (Figure 3A, see "Immunofluorescence staining" in Materials and
111 methods). In brief, we crossed the *Drosophila melanogaster* line expressing a reporter mRNA containing MS2
112 stem loops driven by the *cis*-regulatory region of *hb* to another line that contains MCP-GFP to label the mRNA
113 with GFP. The mRNA transcription signal was then amplified using IF, in conjunction with staining for histone
114 modifications (Figure 3B-E for H3K4me1 and H3K27me3). The *hb* transcription sites appeared in a radial band
115 toward the anterior of stage 5 embryos and in neuroblasts that would become the ventral nerve cord in stage
116 10 embryos.

117 To quantify the spatial distribution of histone marks around transcription sites, we computed the
118 average radial intensity distribution function centered on the transcription site (Figure 3F-J), using the method
119 described in (Tsai et al., 2017) , also see "Image processing" in Materials and methods. The histone
120 environment around *hb* transcription sites showed changes that deviated from the global trend presented in
121 Figure 2. Specifically, we observed a clear increase in H3K4me1 around *hb* transcription sites going from stage
122 5 to stage 10 (Figure 3F), while H3K4me3 (Figure 3G) only showed a small increase. This is the opposite for
123 their global distributions (Figure 2F & G). H3K27ac (Figure 3H) did not change between stage 5 and 10, but
124 H3K36me3 (Figure 3I) intensity showed a moderate increase. Interestingly, many histone modifications

125 showed an initial dip in intensity up to 200-300 nm from the transcription sites. The repressive mark
126 H3K27me3 (Figure 3J) showed a different functional form, with no initial dip and a gentle downward slope.
127 There were no changes between stages 5 and 10, despite the strong increase in H3K27me3 throughout the
128 nucleus going from stage 5 to 10 (Figure 2J). The specific increase in H3K4me1 could indicate the inclusion of
129 more distal regulatory elements in older embryos. The relatively unchanged H3K4me3 profile suggests that
130 proximal regulatory elements are in use in both the early and late stages of development.

131 Spatially dependent changes in the local histone environment at *rho* transcription sites

132 As we observed changes in the local histone environment as a function of time, we investigated if the
133 local histone modification levels could also have spatial dependence on the location of the cell. The *rho* enhancer
134 drives expression in an anterior to posterior band along the side of stage 5 embryos (Figure 4A). The sharp ventral
135 edge of the *rho* pattern results from Snail repression and the pattern trails off gradually in the dorsal direction due
136 to a decreasing gradient of the activator Dorsal (Figure 4B). While most transcriptionally active cells are in the
137 active region (Figure 4C, Active), some nuclei expressing from the *rho* enhancer could still be observed in the
138 repressed region (Figure 4C, Rep.) using a similar method for imaging *hb* transcription and histone modifications
139 (see "Fly lines" in Materials and methods).

140 We quantified H3K4me1 and H3K4me3 at *rho* transcription sites (Figure 4D), sorting cells based on their
141 location in the *rho* expression pattern (e.g. Figure 4E & F). We observed that transcription sites in the active region
142 had a higher level of H3K4me1 compared to sites in the repressed region (Figure 4G, $p < 0.05$, two-tailed Student's
143 t-test). In contrast, there was no difference for H3K4me3 (Figure 4H). While the difference in H3K4me1 could be
144 due to regulatory actions from the *rho* enhancer due to the levels of the Snail repressor, H3K4me3 levels could be
145 explained by the reporter construct containing a poised promoter. Thus, our results show that local histone
146 modifications could report on the state of regulatory elements, which may differ depending on the time and place
147 of expression, even for the same gene.

Increasing heterogeneity in the nucleus could be an integral part of embryogenesis

During development, the embryo undergoes changes in its transcriptional profiles, adapting to different regulatory needs (Figure 4I & J). In early embryos, cell division occur quickly and transcription factors form gradients spanning the embryo with uniform intra-nuclear distributions (Figure 4I). This early stage lasts approximately 6 hours in *D. melanogaster* embryos. Subsequently, the division rate slows down and the detailed segmentation of the body takes place. This phase lasts several times longer, requiring approximately 18 hours. During this phase, many regulatory and signaling pathways in different cell types and organs become active, leading to a complicated regulatory environment in the nucleus (Figure 4J). We observed that the expression patterns of transcription factors became cell-specific and their distributions within the nucleus, heterogeneous. For transcription factors that could regulate different genes during later stages of development, physical separation from early genes in the nucleus can prevent inadvertent crosstalk.

As transcription factor interacts with DNA, this partitioning of their nuclear distribution could reflect a change in the chromatin environment. Starting from when zygotic gene expression turns on, the levels of histone modifications rapidly increase in specific places on the genome. This occurs concurrent to the establishment of higher order structures, such as topologically associating domains (TADs) and to the chromatin organizing into distinct transcriptionally active or repressed regions. We observed such increases in active and repressive histone modifications in post zygotic transition embryos. The increase in H3K27me3, associated with the polycomb group proteins (Denholtz et al., 2013), was the most drastic, which could be differentiating cells shutting down genomic regions. This change in chromatin organization could create distinct accessibility patterns, guiding transcription factors into heterogeneous distributions in older embryos.

These changes in the distributions of transcription factors and chromatin states could alter the regulation of genes depending on the timing of their expression. For example, we observed an increase in H3K4me1 near active *hb* transcription sites between stage 5 and 10 embryos. In contrast, the levels of H3K4me3 were high in both younger and older embryo. The rapid division cycle and relative lack of structure in the nucleus in the early embryo might mean that genes preferentially utilize proximal regulatory elements due to kinetic constraints. As the

174 nuclear environment becomes more stable and heterogeneous in older embryos, long-distance interactions could
175 form and introduce distal regulatory elements. For genes active during multiple developmental stages, this
176 permits them to respond to different regulatory inputs and serve multiple roles using the same *cis*-regulator
177 region. Moreover, we observed a similar trend in space for the transcription sties from the *rho* enhancer,
178 where changing H3K4me1 but constant H3K4me3 suggests a shared active promoter but differential
179 engagement from enhancers. Together, these results imply that the local histone environments around genes
180 could be associated with the states of different *cis*-regulatory elements. These differences could refine the
181 expression pattern over time, as is the case for many developmental genes (Briscoe and Small, 2015), where
182 differences in local epigenetic marking could guide incorrectly expressing or silent cells into their proper state.

183 This survey of the distributions of transcription factors and histone modifications in *Drosophila*
184 embryos has provided evidence for the emergence of a heterogeneous nucleus during development. In a way,
185 this nuclear process mirrors the increasingly complex patterns that control morphogenesis across the entire
186 embryo. This shift in the nuclear environment highlights the need to investigate gene regulation beyond the
187 switchover to zygotic expression and even gastrulation. Lineage-, location-, and time-specific observation of
188 the environments around individual genes could yield insights into how regulatory mechanisms may differ
189 between older and younger embryo. Changes in heterogeneity across different length scales could be a
190 hallmark of embryo development and other regulatory processes in eukaryotes.

191 Materials and methods

192 Fly lines

193 All *Drosophila melanogaster* strains were maintained under standard laboratory conditions at 23 °C. *D.*
194 *melanogaster* containing the *cis*-regulatory region of *hunchback* (*hb*) on a bacterial artificial chromosome (BAC)
195 driving a *yellow* reporter mRNAs containing 24 MS2 stem loops generated in (Bothma et al., 2015) was used as a
196 readout for the expression of *hb*. The reporter construct for *rho* is derived from the plasmid pIB-hbP2-P2P-lacZ-
197 αTub3 UTR (Chen et al., 2012) with the hbP2 region between the restriction sites HindIII and AscI replaced with the
198 *rhoNEE* sequence. The plasmid was synthesized by Genscript (Piscataway, New Jersey, USA). The construct was

199 injected into Bloomington Drosophila Stock Center line 27388 and integrated using RMCE by GenetiVision
200 (Houston, Texas, USA). Virgin flies from a transgenic *D. melanogaster* line containing MS2 coat protein (MCP) fused
201 with eGFP driven by the *nanos* promoter from (Garcia et al., 2013) was crossed with the *hbBAC* or the *rho* reporter
202 line to label the transcriptions sites for further amplification using immunofluorescence (IF) staining. The MCP-GFP
203 line does not contain a nuclear localization signal (NLS) to minimize MCP-GFP forming aggregates in the nucleus in
204 the absence of MS2 mRNAs.

205 Enhancer sequence for *rhoNEE*

206 CTTGGGCAGGATGGAAAAATGGGAAAACATGCGGTGGGAAAAACACACATCGCGAAACATTTGGCGCAACTTGCGGAAGAC
207 AAGTGCGGCTGCAACAAAAAGTCGCGAAACGAAACTCTGGGAAGCGGAAAAAGGACACCTTGCTGTGCGGCGGGAAGCGCA
208 AGTGGCGGGCGGAATTTCCTGATTCGCGATGCCATGAGGCACTCGCATATGTTGAGCACATGTTTTGGGGGAAATTCCCGGGC
209 GACGGGCCAGGAATCAACGTCCTGTCCTGCGTGGGAAAAGCCCACGTCCTACCCACGCCCACTCGGTTACCTGAATTCGAGCT

210 Immunofluorescence staining

211 Embryos from w^{1118} flies (for imaging transcription factors) and from crosses of the *hbBAC* or *rho* reporter line with
212 the MCP-GFP line (for imaging transcription sites and histone modifications) were collected, fixed and stained
213 using the protocols in (Crocker et al., 2015; Tsai et al., 2017). Primary antibodies were detected using secondary
214 antibodies labeled with Alexa Fluor dyes (at a dilution ratio of 1:500, Invitrogen) for confocal and Airyscan imaging.
215 Transcription sites, Hb and Kr were imaged using Alexa488 and the rest with Alexa555. For STED microscopy,
216 secondary antibodies with Alexa594 (1:500, Invitrogen) or STAR RED (1:250, Abberior) were used. Ubx was imaged
217 using Alexa594 and the rest using STAR RED.

218 The primary antibodies and their dilution ratios were:

219 Hb: Generated for the Berkeley Drosophila Transcription Network Project (Li et al., 2008), (1:100)

220 Kr: Generated for the Berkeley Drosophila Transcription Network Project (Li et al., 2008), (1:100)

221 Ubx: Developmental Studies Hybridoma Bank, FP3.38-C, (1:20)

222 En: Santa Cruz Biotechnology, (d-300), sc-28640, (1:50)

223 GFP: ThermoFisher, GFP Monoclonal Antibody (3E6), A-11120, (1:500)

224 H3K4me1: Merck, Anti-monomethyl-Histone H3 (Lys4) Antibody, 07-436, (1:250)

225 H3K4me3: Cell-Signaling Technology, Tri-Methyl-Histone H3 (Lys4) (C42D8) Rabbit mAb, 9751, (1:250)

226 H3K27ac: Active Motif, Histone H3K27ac antibody (pAb), 39133, (1:250)

227 H3K27me3: Active Motif, Histone H3K27me3 antibody (pAb), 39157, (1:250)

228 H3K36me3: abcam, Anti-Histone H3 (tri methyl K36) antibody, ab194677, (1:250)

229 Confocal and Airyscan microscopy

230 Confocal and Airyscan imaging follow the protocols in (Tsai et al., 2017). Specifically, mounting of fixed Drosophila
231 embryos was done in ProLong Gold + DAPI (Molecular Probes, Eugene, OR). Fixed embryos at the appropriate
232 stage and orientation were imaged on a Zeiss LSM 880 confocal microscope with FastAiryscan (Carl Zeiss
233 Microscopy, Jena, Germany). Excitation lasers with wavelengths of 405, 488 and 561 nm were used as appropriate
234 for the specific fluorescent dyes. Whole-embryo overviews were imaged using a Zeiss LD LCI Plan-Apochromat
235 25x/0.8 Imm Korr DIC M27 objective. High resolution confocal and Airyscan stacks were imaged using a Zeiss Plan-
236 Apochromat 63x/1.4 Oil DIC M27 objective. The optimal resolution as recommended by the Zen software from
237 Zeiss was used for the x-y (70.6 nm for confocal and 42.5 nm for Airyscan) and z direction (320 nm for confocal and
238 190 nm for Airyscan) of stacks used for quantification. The laser power and gain were adjusted to maximize the
239 signal to noise ratio within the dynamic range of the PMT or Airyscan detector. The acquired Airyscan stacks were
240 processed with Zen 2.3 SP1 (Carl Zeiss Microscopy, Jena, Germany) in 3D mode to obtain super-resolved images.

241 STED microscopy

242 Mounting of fixed Drosophila embryos was done in ProLong Diamond without DAPI (Molecular Probes, Eugene,
243 Oregon, USA). Fixed embryos at the appropriate stage and orientation were imaged on a STEDYCON (Abberior
244 Instruments, Göttingen, Germany) in 2D STED mode on an Olympus BX53 microscope (Olympus, Tokyo, Japan).
245 Excitation lasers with wavelengths of 594 and 640 nm were used as appropriate for the specific fluorescent dyes.
246 The wavelength of the STED laser was 775 nm. All samples were imaged using an Olympus UPlanSApo 100X Oil/1.4
247 objective. The resolutions used for the x-y and z direction were 25 nm and 250 nm, respectively. The laser power
248 and gain were adjusted to maximize the signal to noise ratio within the dynamic range of the APD detector on the
249 STEDYCON.

Image processing

Image processing was done using Fiji (Schindelin et al., 2012) with the 3D ImageJ Suite plugin (Schmid et al., 2010). Image processing to obtain radially averaged intensity distributions around transcription sites was done according to (Tsai et al., 2017), with the following modification to signal normalization: for each transcription site, the maximum intensity measured in the entire radial distribution is normalized to 1, instead of normalizing to the intensity value at $r = 0$. Radially averaged autocerrelation functions were computed using an ImageJ macro (imagejdocu.tudor.lu/macro/radially_averaged_autocorrelation). AiryScan images were used for their wider field of view compared to STED, in order to include a larger number of nuclei. Intensity distributions and autocorrelation fuctions were plotted using Matlab (MathWorks, Natick, MA).

Acknowledgements

The *hunchback* BAC line was a generous gift from Michael Levine. The MCP-eGFP line and the plasmid pIB-hbP2-P2P-lacZ-αTub3 UTR were generous gifts from Hernan Garcia. The Hunchback and Krüppel primary antibody were generous gifts from Mark Biggin. We would like to thank Marko Lampe at the EMBL Advanced Light Microscopy Facility for his expert advice and training to conduct STED imaging. We would also like to thank members of the Crocker Group for valuable discussions and suggestions to improve the manuscript.

Funding

Albert Tsai is supported by the German Research Foundation (Deutsche Forschungsgemeinschaft, TS 428/1-1). Albert Tsai and Justin Crocker are supported by the European Molecular Biology Laboratory (EMBL).

Data and Material Availability

The original images (AiryScan, confocal, and STED) will be available for download and are indexed at: https://www.embl.de/download/crocker/XXXXX. All fly lines and plasmid sequences will be available upon reasonable request.

References

Bintu, B., Mateo, L.J., Su, J.H., Sinnott-Armstrong, N.A., Parker, M., Kinrot, S., Yamaya, K., Boettiger, A.N., and Zhuang, X. (2018). Super-resolution chromatin tracing reveals domains and cooperative interactions in single cells. Science (80-.). *362*.

Boettiger, A.N., Bintu, B., Moffitt, J.R., Wang, S., Beliveau, B.J., Fudenberg, G., Imakaev, M., Mirny, L.A., Wu, C., and Zhuang, X. (2016). Super-resolution imaging reveals distinct chromatin folding for different epigenetic states. Nature *529*, 418–422.

Bothma, J.P., Garcia, H.G., Ng, S., Perry, M.W., Gregor, T., and Levine, M. (2015). Enhancer additivity and non-additivity are determined by enhancer strength in the Drosophila embryo. Elife *4*.

Briscoe, J., and Small, S. (2015). Morphogen rules: design principles of gradient-mediated embryo patterning. Development *142*, 3996–4009.

Chen, H., Xu, Z., Mei, C., Yu, D., and Small, S. (2012). A System of Repressor Gradients Spatially Organizes the Boundaries of Bicoid-Dependent Target Genes. Cell *149*, 618–629.

Chen, H., Levo, M., Barinov, L., Fujioka, M., Jaynes, J.B., and Gregor, T. (2018). Dynamic interplay between enhancer–promoter topology and gene activity. Nat. Genet. *50*, 1296–1303.

Consortium, T.E.P. (2012). An integrated encyclopedia of DNA elements in the human genome. Nature *489*, 57–74.

Crocker, J., Abe, N., Rinaldi, L., McGregor, A.P.P., Frankel, N., Wang, S., Alsawadi, A., Valenti, P., Plaza, S., Payre, F., et al. (2015). Low affinity binding site clusters confer hox specificity and regulatory robustness. Cell *160*, 191–203.

Denholtz, M., Bonora, G., Chronis, C., Splinter, E., de Laat, W., Ernst, J., Pellegrini, M., and Plath, K. (2013). Long-range chromatin contacts in embryonic stem cells reveal a role for pluripotency factors and polycomb proteins in genome organization. Cell Stem Cell *13*, 602–616.

Furlong, E.E.M., and Levine, M. (2018). Developmental enhancers and chromosome topology. Science (80-.). *361*, 1341–1345.

Garcia, H.G., Tikhonov, M., Lin, A., and Gregor, T. (2013). Quantitative Imaging of Transcription in Living Drosophila Embryos Links Polymerase Activity to Patterning. Curr. Biol. *23*, 2140–2145.

Johnson, D.S., Mortazavi, A., Myers, R.M., and Wold, B. (2007). Genome-Wide Mapping of in Vivo Protein-DNA Interactions. Science (80-.). *316*, 1497–1502.

Kundaje, A., Meuleman, W., Ernst, J., Bilenky, M., Yen, A., Heravi-Moussavi, A., Kheradpour, P., Zhang, Z., Wang, J., Ziller, M.J., et al. (2015). Integrative analysis of 111 reference human epigenomes. Nature *518*, 317–330.

Li, X., MacArthur, S., Bourgon, R., Nix, D., Pollard, D.A., Iyer, V.N., Hechmer, A., Simirenko, L., Stapleton, M., Hendriks, C.L.L., et al. (2008). Transcription Factors Bind Thousands of Active and Inactive Regions in the Drosophila Blastoderm. PLoS Biol. *6*, e27.

Lim, B., Heist, T., Levine, M., and Fukaya, T. (2018). Visualization of Transvection in Living Drosophila Embryos. Mol. Cell *70*, 287-296.e6.

Long, H.K., Prescott, S.L., and Wysocka, J. (2016). Ever-Changing Landscapes: Transcriptional Enhancers in Development and Evolution. Cell *167*, 1170–1187.

308 Mallo, M., and Alonso, C.R. (2013). The regulation of Hox gene expression during animal development.
309 Development *140*, 3951–3963.

310 Mateo, L.J., Murphy, S.E., Hafner, A., Cinquini, I.S., Walker, C.A., and Boettiger, A.N. (2019). Visualizing DNA folding
311 and RNA in embryos at single-cell resolution. Nature *568*, 49–54.

312 Mir, M., Reimer, A., Haines, J.E., Li, X.-Y., Stadler, M., Garcia, H., Eisen, M.B., and Darzacq, X. (2017). Dense Bicoid
313 hubs accentuate binding along the morphogen gradient. Genes Dev. *31*, 1784–1794.

314 Mir, M., Stadler, M.R., Ortiz, S.A., Hannon, C.E., Harrison, M.M., Darzacq, X., and Eisen, M.B. (2018). Dynamic
315 multifactor hubs interact transiently with sites of active transcription in Drosophila embryos. Elife *7*.

316 Reiter, F., Wienerroither, S., and Stark, A. (2017). Combinatorial function of transcription factors and cofactors.
317 Curr. Opin. Genet. Dev. *43*, 73–81.

318 Schindelin, J., Arganda-Carreras, I., Frise, E., Kaynig, V., Longair, M., Pietzsch, T., Preibisch, S., Rueden, C., Saalfeld,
319 S., Schmid, B., et al. (2012). Fiji: an open-source platform for biological-image analysis. Nat Methods *9*, 676–682.

320 Schmid, B., Schindelin, J., Cardona, A., Longair, M., and Heisenberg, M. (2010). A high-level 3D visualization API for
321 Java and ImageJ. BMC Bioinformatics *11*, 274.

322 Shema, E., Bernstein, B.E., and Buenrostro, J.D. (2019). Single-cell and single-molecule epigenomics to uncover
323 genome regulation at unprecedented resolution (Nature Publishing Group).

324 Spitz, F., and Furlong, E.E.M. (2012). Transcription factors: from enhancer binding to developmental control. Nat.
325 Rev. Genet. *13*, 613–626.

326 Stunnenberg, H.G., International Human Epigenome Consortium, S., Hirst, M., Almeida, M. de, Altucci, L., Amin, V.,
327 Amit, I., Antonarakis, S.E., Aparicio, S., Arima, T., et al. (2016). The International Human Epigenome Consortium: A
328 Blueprint for Scientific Collaboration and Discovery. Cell *167*, 1145–1149.

329 Szabo, Q., Jost, D., Chang, J.M., Cattoni, D.I., Papadopoulos, G.L., Bonev, B., Sexton, T., Gurgo, J., Jacquier, C.,
330 Nollmann, M., et al. (2018). TADs are 3D structural units of higher-order chromosome organization in Drosophila.
331 Sci. Adv. *4*, eaar8082.

332 Tanay, A., and Regev, A. (2017). Scaling single-cell genomics from phenomenology to mechanism. Nature *541*,
333 331–338.

334 Thurman, R.E., Rynes, E., Humbert, R., Vierstra, J., Maurano, M.T., Haugen, E., Sheffield, N.C., Stergachis, A.B.,
335 Wang, H., Vernot, B., et al. (2012). The accessible chromatin landscape of the human genome. Nature *489*, 75–82.

336 Tsai, A., Muthusamy, A.K.A.K., Alves, M.R.P.M.R., Lavis, L.D.L.D., Singer, R.H.R.H., Stern, D.L.D.L., and Crocker, J.
337 (2017). Nuclear microenvironments modulate transcription from low-affinity enhancers. Elife *6*.

338

339 # Figures

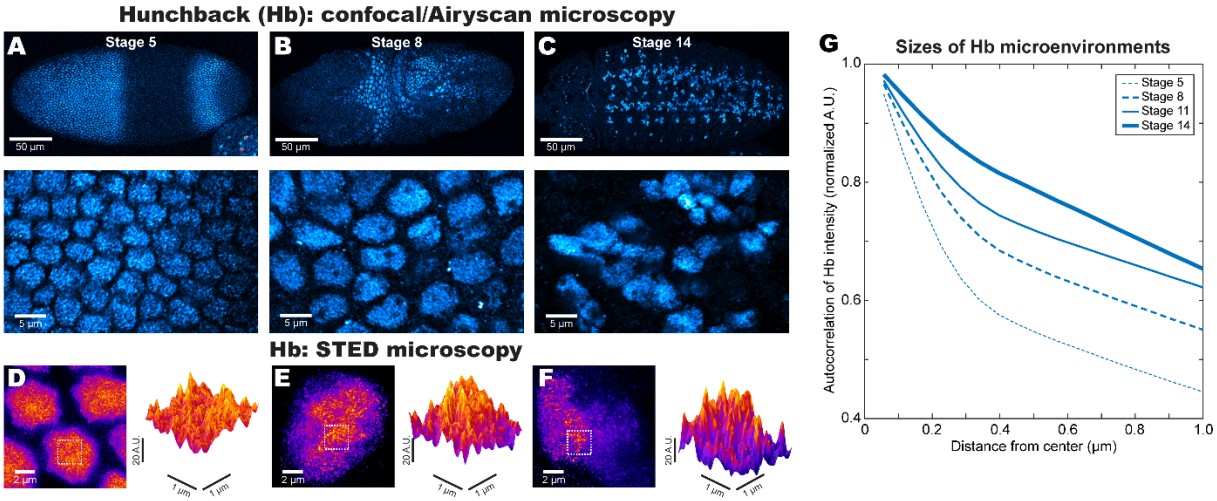

341 ## Figure 1: Increasing heterogeneity in Hb distribution as embryo development progresses

342 The distribution of Hb in *Drosophila* embryos becomes increasingly cell-specific from stage 5 (A, top panel), to
343 stage 8 (B, top panel), and to stage 14 (C, top panel). The bottom panels in A-C show a zoomed-in view of the
344 nuclear distribution of Hb using AiryScan. STED microscopy (D-F) shows that the levels of Hb are high and uniform
345 across the nucleus in stage 5 (D), but becomes increasingly heterogeneous through stage 8 (E) and stage 14 (F). (G)
346 The radially averaged autocorrelation function of Hb quantifies the overall prevalence of spatial structures at
347 different length scales.

348

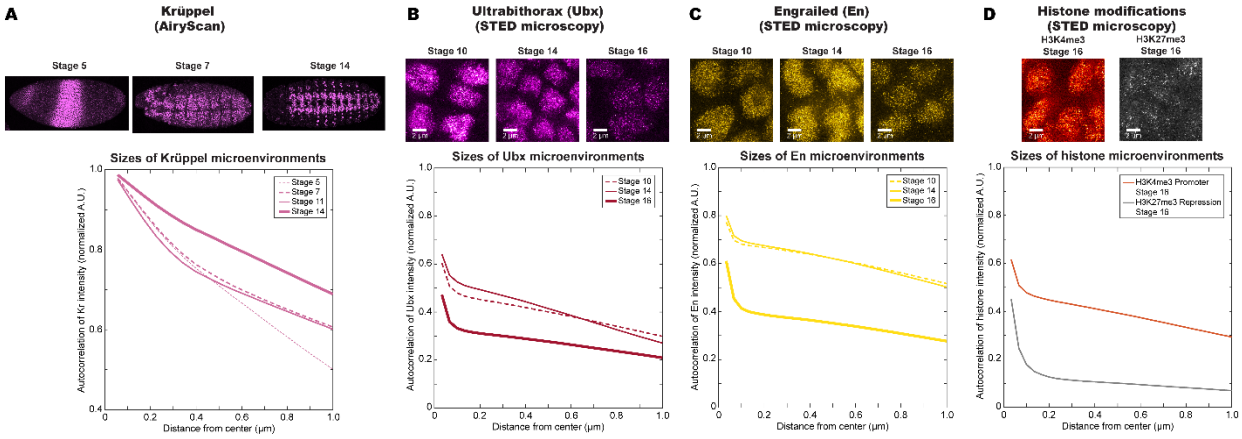

Figure S1: The spatial scales of transcription factors and histone marks as a function of embryo age and regulatory function

(A) An increase in the autocorrelation function is also observed for Krüppel across developmental stages. Transcription factors that are only expressed during later stages of embryo development, such as (B) Ubx and (C) En, do not show a uniform nuclear distribution. During stages 10 and 14, when both factors are expressed, their distributions are heterogeneous and show significant levels of autocorrelation. Their expression decreases significantly by stage 16. (D) The physical sizes of the chromatin can vary according to their transcriptional state.

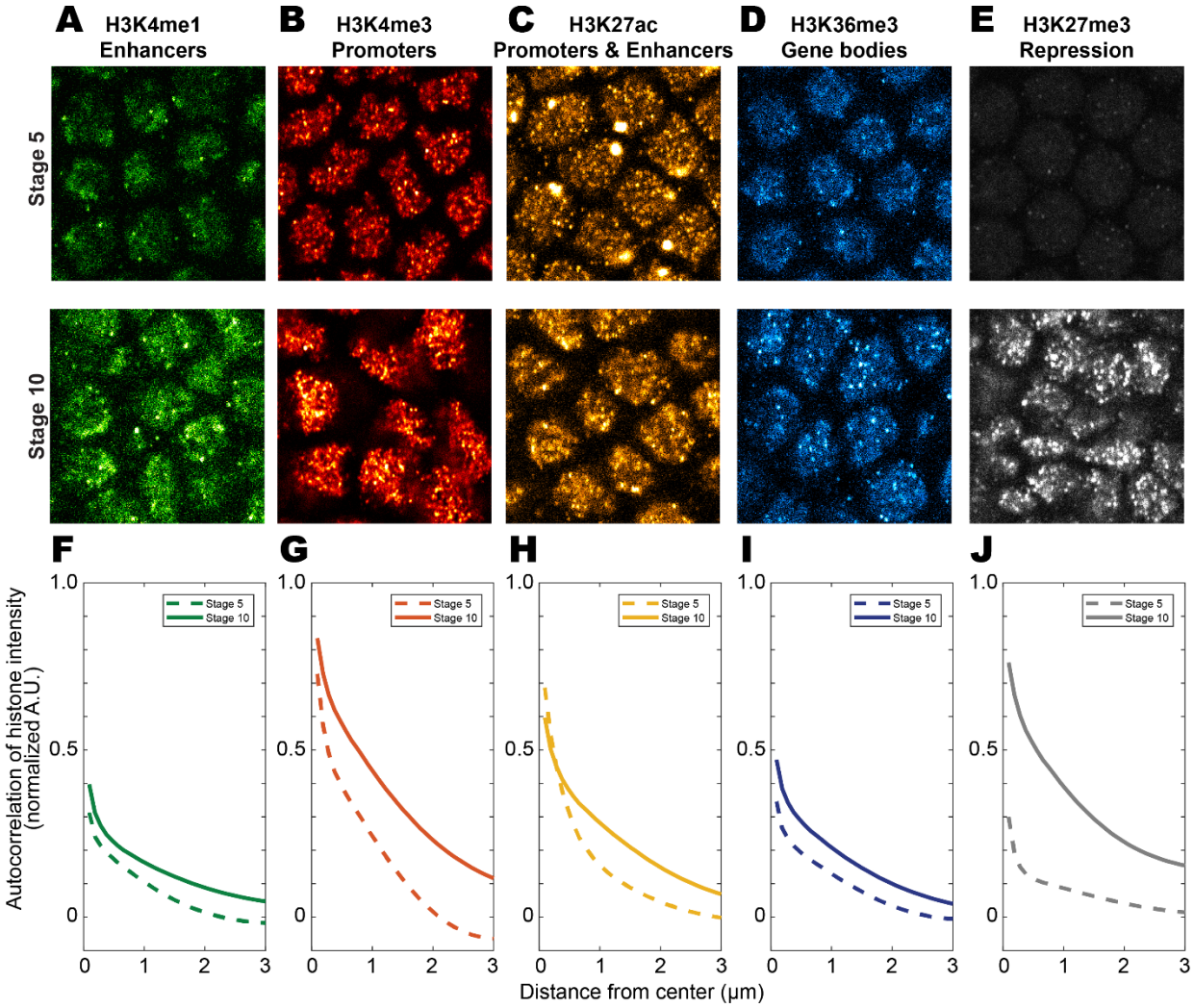

Figure 2: Increasing histone modifications as a function of embryo age

The chromatin shows increased levels of histone modifications as shown in (A-E) when comparing embryos at stages 5 and 10: (A) H3K4me1 marking enhancers, (B) H3K4me3 marking promoters, (C) H3K27ac marking active enhancers and promoters, (D) H3K36me3 marking active gene bodies, and (E) H3K27me3 marking repressed regions. The autocorrelation functions (F-J) of the histone modifications shows this general trend, with an increase in association across all length scales.

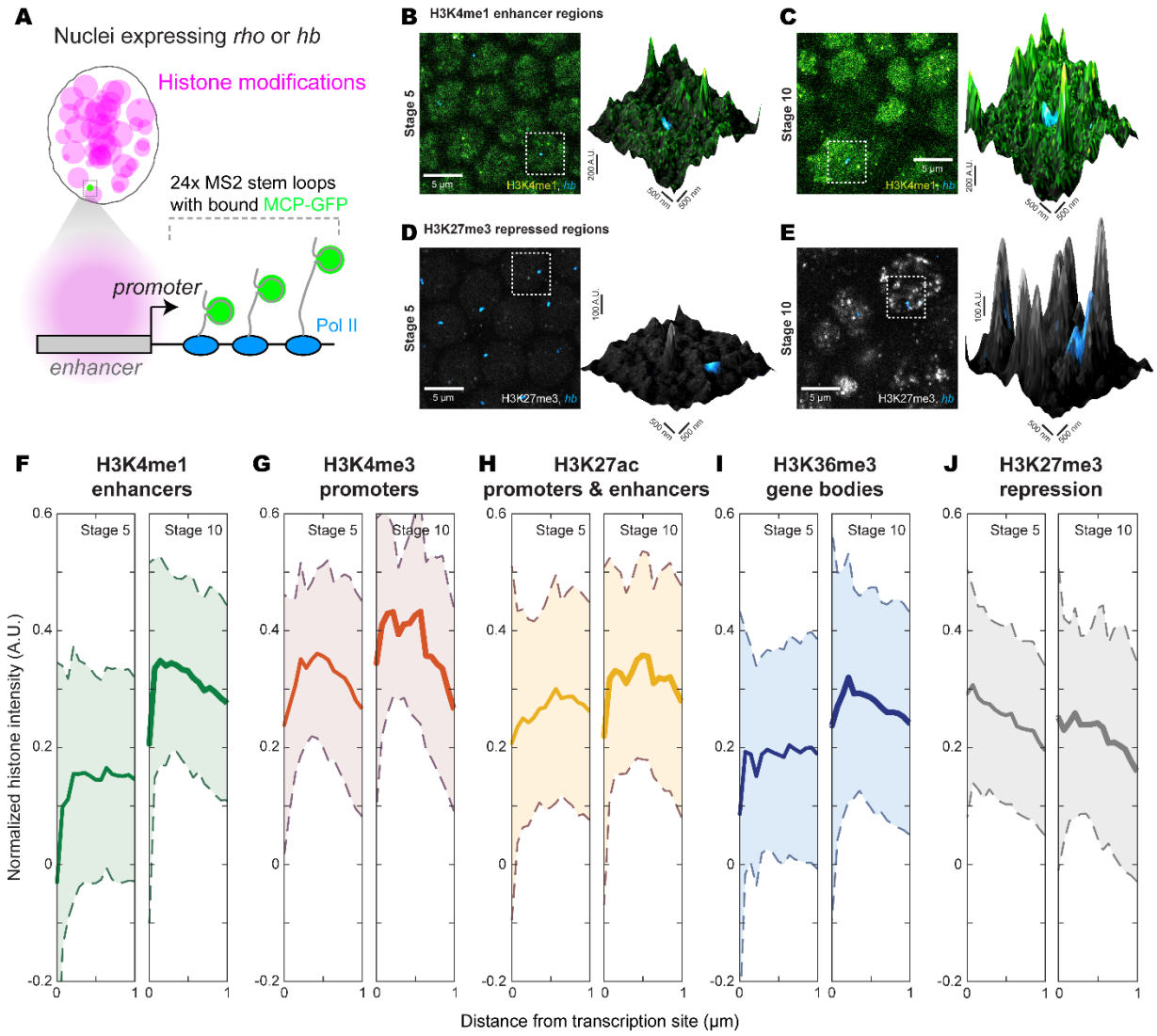

366 Figure 3: The histone environment at *hb* transcription sites depends on the timing of

367 their expression

368 (A) Marking transcription sites of a MS2 reporter gene driven by the *cis*-regulatory region of *hb* or *rho* using MCP-

369 GFP and IF amplification preserves the signal of histone modifications stained using IF. This allows the

370 simultaneous imaging of transcription sites and histone modifications with good signal-to-noise ratio (B & C for

371 H3K4me1 and D & E for H3K27me3, at stage 5 and 10 respectively). (F-J) The radially averaged distributions of

372 histone modifications around *hb* transcription sites show locally specific changes between stages 5 and 10.

373 H3K4me1: stage 5 n = 51 transcription sites, stage 10 n = 111. H3K4me3: stage 5 n = 69, stage 10 n = 52. H3K27ac:

374 stage 5 n = 178, stage 10 n = 63. H3K36me3: stage 5 n = 54, stage 10 n = 88. H3K27me3: stage 5 n = 235, stage 10 n

375 = 66.

376

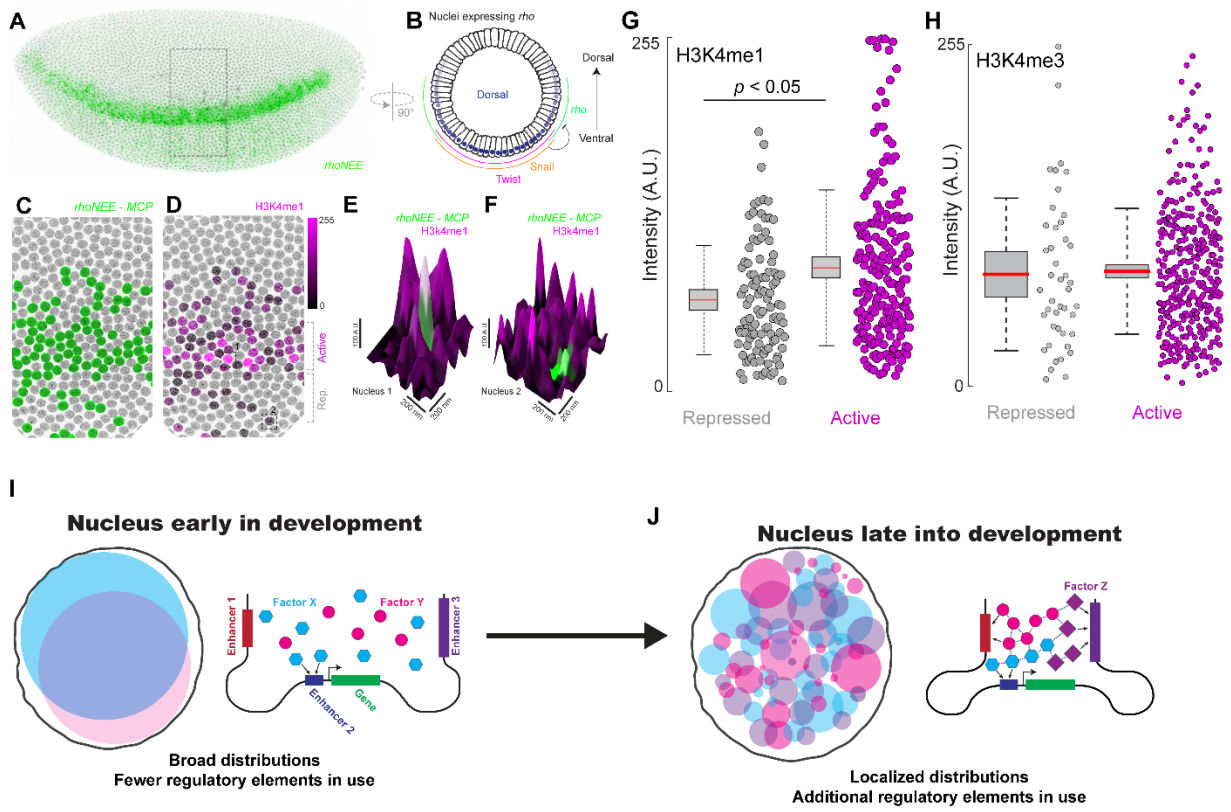

Figure 4: The histone environment at *rho* transcription sites depends on their location in the embryo

(A) The expression pattern of the *rhoNEE* enhancer on a side view of a stage 5 embryo. (B) The regulatory inputs of *rho* along the dorsal-ventral axis. (C) Zoomed panel from the box in (A) with nuclei with *rho* transcription site in green. (D) Same view as (C) with the shade of magenta depicting the intensity of H3K4me1 at the transcription site. (E & F) Zoomed in view around a transcription of a nucleus from the (E) active and (F) repressed zone of *rho* expression, with the z-axis showing H3K4me1 intensity. (G & H) Quantification of (G) H3K4me1 and (H) H3K4me3 levels at *rho* transcription sites. H3K4me1 repressed: n = 94 transcription sites, active: n = 535. H3K4me3 repressed: n = 44, active n = 354. (I) The nuclear environment in early embryo development is more uniform and gene regulation may preferentially occur using proximal elements. (J) The nucleus is heterogeneous in older embryos and more distal regulatory elements may be engaged in transcriptional microenvironments.